Energy Equip. Sys./ Vol. 12/No. 1/March 2024/ 29-45

ENERGY EQUIPSYS

Energy Equipment and Systems

http://energyequipsys.ut.ac.ir
www.energyequipsys.com

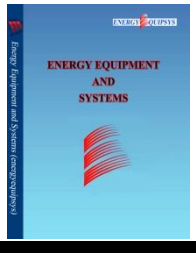

Comprehensive performance evaluation and multi-criteria optimization of a novel tri-generation system based on geothermal energy

Authors

Nima Ghasemzadeh[a*]
Ramin Ghiami Sardroud[b]
Ehsan Gholamian[a]
Mortaza Yari[a*]

[a] Department of Mechanical Engineering, Faculty of Mechanical Engineering, University of Tabriz, Tabriz, Iran

[b] Faculty of Mechanical Engineering, Sahand University of Technology, Sahand New Town, Tabriz, Iran

Article history:
Received : 13 July 2023
Accepted : 4 September 2023

ABSTRACT

A novel tri-generation system powered by geothermal energy is assessed from exergo-economic and thermodynamic perspectives. The proposed system consists of a geothermal single flash cycle, an ORC with the OFOH and the IHE, a HDH desalination system, and a double-effect absorption refrigeration system. This system aims to produce power, cooling load, and the freshwater. The design parameters effects such as geothermal inlet temperature, the flash chamber inlet pressure, HPG temperature difference, and steam-turbine outlet pressure on the main indicators, including exergy efficiency, cooling load, total product unit cost, and produced freshwater mass flow rate. Moreover, the multi-objective optimization is applied using machine learning method and Grey wolf algorithm to optimize the total product unit cost, the net generated power rate, and the exergy efficiency. Under base design conditions, the total product unit cost and the exergy efficiency are 77.8 $/GJ and 44.2%, respectively. Moreover, the results for the exergy efficiency, the total product unit cost, and the net generated power rate of the system under multi-objective optimization are 54%, 62.5 $/GJ, and 180 kW. Among all elements of the current system, TEG1 has the greatest rate of the exergy destruction, which is 94.02 kW. Additionally, the rate of the overall system exergy destruction is 221.72 kW.

Keywords: Tri-generation; Geothermal; Thermo-Economic; Multi-Objective Optimization; Machine Learning; Double-Effect Absorption Refrigeration System; Organic Rankine Cycle.

1. Introduction

As the growing global population grows, there is an increasing demand for energy. However, the current structure of energy consumption heavily relies on fossil fuels, which are limited resources with increasing prices and detrimental effects on the environment. To address this, researchers are exploring alternative strategies, such as renewable energy sources (RES). RESs are responsible for supplying 14% of the total worldwide energy demand [1], and consist of geothermal, solar, hydropower, biomass, and wind energies. Renewable energy sources are able to provide energy services with practically no air pollution and greenhouse gas emissions [1]. Moreover, hydrogen fuels are one of the most

*Corresponding authors: Nima Ghasemzadeh, Mortaza Yari Department of Mechanical Engineering, Faculty of Mechanical Engineering, University of Tabriz, Tabriz, Iran
Email:nimaghasemzadeh98@ms.tabrizu.ac.ir, myari@tabrizu.ac.ir

promising alternative to fossil fuels and can reduce the environmental impacts of fossil fuels [2]. Geothermal energy has mainly three significant uses, including heating systems, producing electricity, and utilizing in the geothermal heat pump [3]. Alavy et al. [4] introduced geothermal based-heat pump as a promising system with no greenhouse gas emissions which is one of the most sustainable heating and cooling systems.

Huang et al. [5] analyzed a trans-critical CO_2 cycle driven by the geothermal cycle using single flash from the viewpoint of exergy evaluation. They carried out both genetic algorithm and Nelder-Mead simplex approach to optimize the exergy efficiency. Based on the findings, the system exergy efficiency under the base design conditions was 32.46%. Utilizing the genetic algorithm and Nelder-Mead simplex approach enhanced the system exergy efficiency to 39.21% and 36.16%, respectively. In another paper, Wang et al. [6] proposed an integrated cycle including the geothermal cycle with single flash and the trans-critical CO_2 cycle. They evaluated this system from energy and exergy perspectives. Referring to the obtained results, the system exergy efficiency, energy efficiency and net power generated were 46.32%, 53.6%, and 401.4 kW, respectively. A thermodynamic assessment, including exergy and energy evaluations, was applied to evaluate the performance of a geothermal cycle with single flash by Assad [7]. Findings depicted that as the separator performs at the mean temperatures of the condenser and well, the highest power can be generated by the turbine. In this system, the expansion valve had the highest exergy destruction. However, the separator operated with exactly zero exergy destruction. Fan et al. [8] suggested a integrated cycle including the two-stage ORC and the geothermal cycle with single flash. They evaluated the combined system from economic, exergy, and energy aspects. In this suggested system, the ORC reused the waste heat of the geothermal system. Using the two-stage ORC to recover the waste heat of single flash geothermal plant increased the system exergy and energy efficiencies by 15.04% and 7.66%, respectively. In addition, employing the two-stage ORC can reduce the system levelized energy cost from 0.125 \$/kW to 0.108 \$/kW. Assad et al. [9] evaluated a integrated single flash cycle and trans-critical CO_2 cycle from exergoeconomic, exergy, and energy aspects. Based on the findings, the greatest exergy destruction rate happened in the CO_2 vapor generator. However, the lowest rate of exergy destruction took place in the geothermal system with single flash. The findings demonstrated that employing the trans-critical CO_2 cycle can enhance the system performances from the viewpoints of the exergy and energy efficiencies.

Due to use of the refrigerants with zero global warming potential and ozone layer depletion potential, absorption cycles have become a promising system for cooling applications. One of the most significant advantages of such systems is that they are capable of utilizing various energy sources, including renewable energies, waste heat of topping cycles, and fossil fuels [10]. The double-effect absorption refrigeration (DEAR) systems are more capable of utilizing energy sources with higher temperature and can reach greater energy efficiencies in comparison to the single-effect absorption systems. Among the various absorption refrigeration cycles, the systems utilizing ammonia-water and water-lithium bromide are considered highly promising. Using waster-lithium bromide mixture as the DEAR system working fluid plays a vitally important role from environmental perspective since it has been reported that the global warming potential and ozone layer depletion potential are zero for lithium bromide solutions [10]. The DEAR system that utilizes water-lithium bromide as the working fluid comprises lithium bromide and water as the absorbent and refrigerant, respectively.

Bagheri et al. [11] evaluated the parallel DEAR system from exergy view point. The highest system exergy efficiency and the exergy efficiency and coefficient of performance were 1.295 and 22.5%, respectively, achieved as the high-pressure generator (HPG) temperatures were 169.6 °C and 142.7 °C, respectively. They also carried out the advanced exergy evaluation. Based on the results of this analysis, the endogenous share of the destroyed exergy is greater than the exogenous share, indicating that it should be focused on the efficiencies of the components to enhance the system performance. In another paper, Garousi et

al. [10] analyzed the reverse parallel, series, and parallel configurations of the DEAR system from exergo-economic, exergy, and energy perspectives. They found that lower investment cost can be achieved as the evaporator and the HPG temperatures are high, but the condenser temperature and the solution heat exchangers' effectiveness are low. Alali et al. [12] evaluated the performance of a system consisting of gas turbine modular helium reactor cycle, DEAR system, and Stirling engine. In this combined cycle, the Stirling engine and the DEAR system reuse the gas turbine cycle waste heat. Employing two bottoming cycles of the Stirling engine and the DEAR system increased the efficiency of energy utilization of the system by 4.73%-5.46%. Moreover, the standalone gas turbine modular helium reactor cycle mass flow rate was 16.1%-17.78% greater than that of the helium. Zhang et al. [13] evaluated a geothermal-based parallel double-effect absorption power cycle from exergy, energy, economic, and environmental viewpoints. They compared the performances of the system with a traditional absorption power system and results revealed that this cycle is able to enhance the system net generated power rate and exergy efficiency by 41.3% and 12.31%, respectively, compared to the traditional absorption power system. Additionally, compared to the traditional absorption power system, the studied system is able to decline the total unit cost by 10.12%. The lowest and greatest exergy destruction belonged to the low-temperature generator and absorber, respectively. Jimenez-Garcia et al. [14] proposed an integrated system including the ORC and the ammonia-lithium nitrate-based DEAR system to meet power and cooling demands. They utilized four different ORC working fluids, consisting of cyclohexane, toluene, benzene, and methanol. The maximum system energy utilization factor and exergy efficiency were 0.854 and 39.82%, respectively, achieved as benzene is employed as the ORC working fluid.

In recent years, researchers have devoted a great deal of effort to introduce cycles that can use the waste heat of topping cycle, and the ORCs have gained significant attention due to their advantages. These cycles are able to generate power by utilizing the low-temperature energy source [15], making them a promising choice for using the waste heat of geothermal energy. Furthermore, these cycles utilize dry working fluids resulting in solving the vapor condensation problem inside the turbine [16]. In addition to mentioned advantages, ORCs can be an appropriate choice to be used as the bottoming cycle due to their ease of maintenance, high reliability and simplicity [17].

Karabuga et al. [18] evaluated a solar powered ORC assisting hydrogen production system from exergy and energy perspectives. The thermal energy generated by solar energy is used by the ORC to produce power, which is then used in the hydrogen production system to produce hydrogen by proton exchange membrane electrolyzer (PEME). The considered two different strategies: the first strategy employed all generated power to produce hydrogen. In this situation, the exergy and energy efficiencies were 2.15% and 3.45%, respectively. In the second strategy, some of the produced power was used for producing hydrogen, resulting in the exergy and energy efficiencies of 0.002% and 0.014%, respectively. In another paper, Ochoa et al. [19] compared the economic, exergy, and energy performances of two bottoming cycles of regenerative ORC and simple ORC to utilize the waste of the supercritical CO_2 simple Brayton cycle. They considered three different ORC working fluids including acetone, toluene, and cyclohexane. From energy and economic perspectives, the best regenerative ORC performances were achieved were achieved as cyclohexane is utilized as the ORC working fluid. For this case, the payback period, the specific investment cost, the levelized cost of energy, and the energy efficiency were 11.2 years, 2626.75 $/kWh, 0.26 $/kWh, and 48.02%, respectively. Javad and Tiwari [20] compared the performances of three different ORCs, including basic, recuperative, and regenerative ORC powered by solar energy from economic and energy aspects. They utilized dodecane, decane, toluene, and nonane as working fluids. The highest generated power was belong to the regenerative ORC, which was 25.23% and 36.6% greater than that for the recuperative and basic ones, respectively. The regenerative ORC achieved the highest energy efficiency of 37.01% by utilizing toluene as the working fluid. Nondy and Gogoi [21] compared the performances of recuperative-regenerative ORC, recuperative ORC, regenerative ORC,

and basic ORC from energy, exergy, and economic perspectives. They also applied multi-objective optimization. Among these four systems, recuperative-regenerative ORC system had the lowest cost rate and highest exergy efficiency. The second and third best systems from exergy and economic viewpoints were regenerative and recuperative ORC systems, respectively. Zhar et al. [22] considered three different layouts of ORC, including basic ORC, regenerative ORC with open feed-heater, and reheating ORC, with distinct working fluids of R152a, R123, isobutene, and R245fa. They applied economic, exergy, and energy analyses to all three cycles. The maximum exergy and energy efficiencies were belong to the regenerative ORC with open feed-heater. From economic viewpoint, the payback period and levelized cost of energy of all three examined ORCs were close to each other.

Humidification dehumidification (HDH) desalination plays a main role in the water purification, and therefore, this technology has attracted much attention. This technology has the economic and environmental advantages, such as the possibility of being driven by renewable energy sources, capability of operating at low temperature, and low maintenance requirements [23].

Abbasi et al. [24] analyzed a tri-generation system from exergy and energy aspects. This system was powered by solid oxide fuel cell (SOFC), and the HDH desalination system and Kalina cycle reused the SOFC waste heat. In addition, the Kalina cycle waste heat was utilized by cold stream of liquefied natural gas. This tri-generation system was proposed to meet cooling, freshwater, and power demands. Based on the results, the system exergy and energy efficiencies were 55% and 60%, respectively. Qasem [25] analyzed the air-heated HDH system utilizing the waste heat of DEAR system from energy and economic perspectives. Under the base design conditions, this system was able to produce cooling effect of 104 and 2100 L/h water with energy utilization factor of 5.9, cooling effect cost of 0.0037 $/kWh, and coefficient performance of 1.2.

To our best knowledge and by surveying the literature, the performance of the studied system has not been yet evaluated. A novel system powered by the geothermal energy has been introduced and assessed from exergy, thermo-economic, and energy perspectives in the current work. Obviously, a good deal of effort has been devoted to finding methods to utilize the geothermal energy. This work aims to employ the geothermal energy waste heat to generate freshwater, power, and cooling. The novel system consists of the geothermal cycle with single flash, the DEAR system, the ORC with the OFOH and the IHE, and the HDH desalination system. To maximize the exergy efficiency and the net output power, and to minimize the system total cost rate based on machine learning method and Grey Wolf algorithm, the multi-objective optimization is conducted.

Nomenclature

Abs	Absorber
$\dot{C}$	Cost rate
COP	Coefficient of performance
$c_{p,tot}$	Unit exergy cost of products
$\dot{E}$	Exergy flow rate
$\dot{E}_D$	Exergy destruction rate
Evap	Evaporator
HDH	Humidification and Dehumidification
HPG	High pressure generator
HX	Heat exchanger
IHE	Internal heat exchanger
LCOE	Levelized cost of Electricity
LPG	Low pressure generator
MOO	Multi − objective optimization
n	Operational years
ORC	Organic Rankine cycle
OFOH	open feed organic fluid heat
P	Pressure
s	Specific entropy
T	Temperature
TEG	Thermo electric generator
$\dot{W}$	Produced/consumed power
Z	Cost function

Subscripts

cv	Control volume
E	Exit
f	Fuel
I	Inlet
p	Products
tot	Total

Superscripts

CI	Capital investment
η	Efficiency

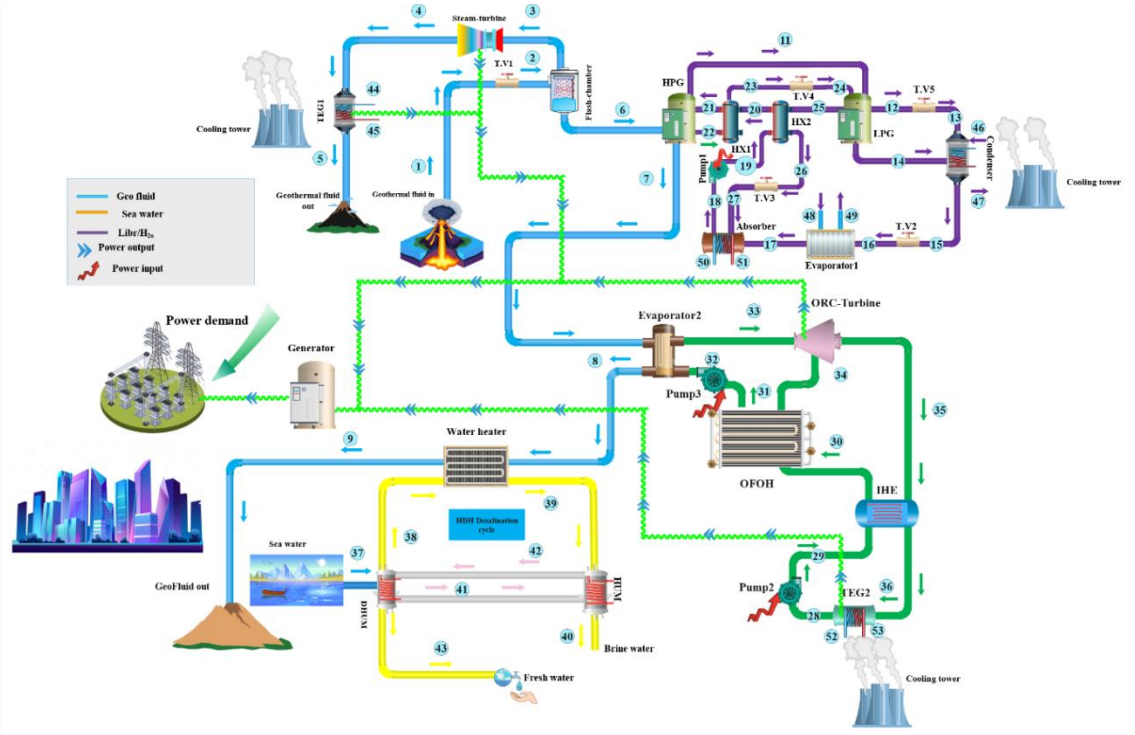

Fig. 1. Schematic diagram of the proposed system

2. System description and assumptions

The studied system schematic diagram is exhibited in Fig. 1.

The proposed cycle includes a single flash geothermal cycle, ORC with an open feed organic fluid heat (OFOH) and an internal heat exchanger (IHE), a DEAR system, and a HDH desalination system. In the single flash geothermal cycle, the geo fluid with high temperature leaves the well (state 1). The saturated geo fluid enters the flash chamber after expanding in valve 1 (state 2). The saturated mixture is divided into two streams. The saturated vapor (state 3) expands and generates power in the steam turbine and then (state 4) enters the thermoelectric power generation 1 (TEG) to generate work. Finally, the geo fluid is injected to the well (state 5). The saturated liquid geo fluid (state 6) leaving the flash chamber enters the HPG to convey heat to the low-temperature water-lithium bromide mixture. The DEAR system consists of four valves, two heat exchangers (HX), high- and low-pressure generators (HPG and LPG), absorber, evaporator, condenser, and a pump. This system uses a heat source to drive a refrigeration system. As mentioned, the HPG is heated by the geo fluid. The ORC includes two pumps, an evaporator, an ORC-Turbine, an IHE, an OFOH, and a TEG 2. In the evaporator 2, the high-temperature geo fluid (state 8) conveys its thermal energy to the ORC working fluid. This high-temperature fluid (state 33) enters ORC-Turbine and produces work. A portion of working fluid leaving the ORC-Turbine (state 34) enters the OFOH, while the remaining portion (state 35) enters the IHE where the heat transfer process takes place. The fluid leaving the IHE (state 36) enters the TEG 2 to produce wok and is then pumped to enter the IHE (state 29). The fluid exiting the IHE (state 30) passes through the OFOH and is pumped to enter the water heater. Finally, the geo fluid is injected to the well (state 9). The thermal energy of geo fluid is transferred to the HDH desalination system to generate freshwater. In this system, the seawater and air circulate in the open and closed circuits, respectively. The process begins with seawater undergoing evaporation with air, and the leftover liquid is released as brine from the humidifier. At the same time, the air is humidified by the humidifier. Eventually, the air leaving the humidifier enters the dehumidifier,

producing distilled water, while the low-temperature air goes back to the humidifier.

2.1. Assumptions

To simplify the process of modelling and simulation, the following assumptions are considered:

1. In evaluation of the proposed cycle, the whole system is considered as steady state.
2. Variations of the kinetic and potential energies during the processes are ignored.
3. Heat transfer in heat exchangers and pressure drop in connecting pipes are omitted.
4. Geothermal fluid input is assumed to be saturated liquid.
5. The distilled water temperature is the average dew point temperature of the incoming air and the temperature of the dry bubble of the outlet air in the dehumidifier [26].

2.2. Input data

In order to evaluate the studied system from thermo-economic and thermodynamic aspects, the required input data are represented in Table 1.

Table 1. The required data for analyzing the proposed system

Parameter	Value	Unit	Reference(s)
T_1	230	°C	[27]
$\dot{m}_1$	2	Kg/s	[27]
P_2	665.5	kPa	[28]
P_4	96.4	kPa	[28]
T_{11}	145	°C	[-]
T_{14}	80	°C	[29]
T_{17}	4	°C	[29]
X_{18}	55.869	%	[29]
T_{28}	40	°C	[28]
T_{33}	120	°C	[28]
P_{29}	581.2	kPa	[28]
T_{39}	348.15	K	[26]
T_{37}	298.15	K	[26]
$\dot{m}_r$	2.233	-	[26]
P_0	101.3	kPa	-
T_0	298.15	K	-

2.3. System thermodynamic modeling

Energy balance and mass conservation for a steady-state control volume are described as:

$$\sum_{inlets}\dot{m}_i = \sum_{outlets}\dot{m}_e \quad (1)$$

$$\dot{Q}_{cv} - \dot{W}_{cv} = \sum_{inlets}\dot{m}_i h_i - \sum_{outlets}\dot{m}_e h_e \quad (2)$$

In the above relations, e and i indicate exits and inlets of the control volume, respectively. Also, the heat transfer rate in the component and the generated/consumed power are denoted as $\dot{Q}_{cv}$ and $\dot{W}_{cv}$, respectively.

To determine the exergy destruction rate of the elements of the proposed system, the exergy balance equation is used. According to Eq.(3), for a control volume operating at steady-state condition, the sum of input exergy flows equals the sum of outflow exergies and the exergy destruction rate.

$$\sum_{inlets}\dot{E}_i + \sum\dot{Q}_j\left(1-\frac{T_0}{T_j}\right) = \sum_{outlets}\dot{E}_e + \dot{W}_{cv} + \dot{E}_{D,cv} \quad (3)$$

In the above relation, the term $\sum_{inlets}\dot{E}_i$ refers to the sum of inlet exergy flows, the term $\sum_{outlets}\dot{E}_e$ refers to the sum of outlet exergy flows, the term $\sum\dot{Q}_j\left(1-\frac{T_0}{T_j}\right)$ denotes the exergy associated with heat transfer of the component, and the term $\dot{E}_{D,cv}$ denotes the exergy destruction rate.

For a working fluid flowing in a control volume, the total exergy flow is equal to the sum of thermomechanical exergy flow and chemical exergy flow, as indicated in Eqs. (4a) to (4c).

$$\dot{E} = \dot{E}_{th} + \dot{E}_{ch} \quad (4.a)$$

$$\dot{E}_{th} = \sum \dot{m}_i \left[\left(h_i - h_0 \right) - T_0 \left(s_i - s_0 \right) \right] \quad (4.b)$$

The exergy balance equations and energy conservation for each of the studied system elements are stated in Table 2.

Table 2. Exergy balance equations and energy conservation of the proposed system elements

Element	Mass and energy balance	Exergy balance
Geothermal subsystem		
T.V1	$(h_1 = h_2)$	$\dot{E}_1 = \dot{E}_2 = \dot{E}_{D,\mathrm{EV1}}$
FC	$\dot{m}_2 h_{12} = \dot{m}_3 h_3 + \dot{m}_6 h_6$ $\dot{m}_{12} = \dot{m}_{14} + \dot{m}_{15}$	$\dot{E}_2 = \dot{E}_3 + \dot{E}_6 + \dot{E}_{D,\mathrm{FC}}$
ST	$\dot{W}_{st1} = \dot{m}_3 (h_3 - h_4)$	$\dot{E}_3 = \dot{E}_4 + \dot{E}_{st} + \dot{E}_{D,\mathrm{st}}$
TEG 1	$\dot{Q}_{TEG1} = \dot{m}_4 (h_4 - h_5)$ $\dot{Q}_{TEG1} = \dot{m}_{44} (h_{45} - h_{44})$	$\dot{E}_4 + \dot{E}_{44} = \dot{E}_5 + \dot{E}_{45} + \dot{W}_{TEG1} + \dot{E}_{D,TEG1}$
double-effect absorption refrigeration subsystem		
HPG	$\dot{Q}_{HPG} = \dot{m}_{22} h_{22} + \dot{m}_{11} h_{11} - \dot{m}_{21} h_{21}$ $\dot{Q}_{HPG} = \dot{m}_{50} (h_{34} - h_{50})$	$\dot{E}_6 + \dot{E}_{21} = \dot{E}_{22} + \dot{E}_{11} + \dot{E}_7 + \dot{E}_{D,\mathrm{HPG}}$
LPG	$\dot{Q}_{LPG} = \dot{m}_{11} h_{11} + \dot{m}_{24} h_{24} - \dot{m}_{14} h_{14} - \dot{m}_{12} h_{12} - \dot{m}_{25} h_{25}$	$\dot{E}_{11} + \dot{E}_{24} = \dot{E}_{12} + \dot{E}_{14} + \dot{E}_{25} + \dot{E}_{D,\mathrm{LPG}}$
Cond	$\dot{Q}_{Cond} = \dot{m}_{13} h_{13} + \dot{m}_{14} h_{14} - \dot{m}_{15} h_{15}$ $\dot{Q}_{Cond} = \dot{m}_{46} (h_{47} - h_{46})$	$\dot{E}_{13} + \dot{E}_{14} + \dot{E}_{46} = \dot{E}_{15} + \dot{E}_{47} + \dot{E}_{D,\mathrm{Cond}}$
Evap1	$\dot{Q}_{Evap1} = \dot{m}_{16} (h_{16} - h_{17})$ $\dot{Q}_{Evap1} = \dot{m}_{48} (h_{49} - h_{48})$	$\dot{E}_{16} + \dot{E}_{48} = \dot{E}_{17} + \dot{E}_{49} + \dot{E}_{D,Evap1}$
Absorber	$\dot{Q}_{Abs} = \dot{m}_{27} h_{27} + \dot{m}_{17} h_{17} - \dot{m}_{18} h_{18}$ $\dot{Q}_{Abs} = \dot{m}_{50} (h_{50} - h_{51})$	$\dot{E}_{17} + \dot{E}_{27} + \dot{E}_{50} = \dot{E}_{18} + \dot{E}_{51} + \dot{E}_{D,\mathrm{Abs}}$
HX2	$\dot{Q}_{HX2} = \dot{m}_{19} (h_{19} - h_{26})$ $\dot{Q}_{HX2} = \dot{m}_{20} (h_{20} - h_{25})$	$\dot{E}_{19} + \dot{E}_{25} = \dot{E}_{20} + \dot{E}_{26} + \dot{E}_{D,\mathrm{HX2}}$
HX2	$\dot{Q}_{HX1} = \dot{m}_{20} (h_{20} - h_{21})$ $\dot{Q}_{HX1} = \dot{m}_{22} (h_{23} - h_{22})$	$\dot{E}_{20} + \dot{E}_{22} = \dot{E}_{21} + \dot{E}_{23} + \dot{E}_{D,\mathrm{HX1}}$
T.V2	$h_{15} = h_{16}$	$\dot{E}_{15} = \dot{E}_{16} + \dot{E}_{D,\mathrm{T.V2}}$
T.V3	$h_{26} = h_{27}$	$\dot{E}_{26} = \dot{E}_{27} + \dot{E}_{D,\mathrm{T.V3}}$
T.V4	$h_{23} = h_{24}$	$\dot{E}_{23} = \dot{E}_{24} + \dot{E}_{D,\mathrm{T.V4}}$
T.V5	$h_{12} = h_{13}$	$\dot{E}_{12} = \dot{E}_{13} + \dot{E}_{D,\mathrm{T.V5}}$
Pump1	$\dot{W}_{Pump1} = \dot{m}_{18} (h_{19} - h_{18})$	$\dot{E}_{18} + \dot{W}_{Pump1} = \dot{E}_{19} + \dot{E}_{D,\mathrm{pump1}}$
HDH desalination subsystem		
Water heater	$\dot{Q}_{Water\ heater} = \dot{m}_8 (h_8 - h_9)$ $\dot{Q}_{Water\ heater} = \dot{m}_{38} (h_{39} - h_{38})$	$\dot{E}_8 + \dot{E}_{38} = \dot{E}_9 + \dot{E}_{39} + \dot{E}_{D,\mathrm{Waterheater}}$
Hum	$\dot{m}_{39} h_{39} + \dot{m}_{41} h_{41} = \dot{m}_{40} h_{40} + \dot{m}_{42} h_{42}$ $\dot{m}_{31} + \dot{m}_{29} = \dot{m}_{30} + \dot{m}_{32}$	$\dot{E}_{39} + \dot{E}_{41} = \dot{E}_{40} + \dot{E}_{42} + \dot{E}_{D,\mathrm{Hum}}$
Dhum	$\dot{m}_{37} h_{37} + \dot{m}_{42} h_{42} = \dot{m}_{38} h_{38} + \dot{m}_{43} h_{43}$ $\dot{m}_{33} = \dot{m}_{43} (\omega_{42} - \omega_{41})$	$\dot{E}_{37} + \dot{E}_{42} = \dot{E}_{38} + \dot{E}_{43} + \dot{E}_{D,\mathrm{Dhum}}$
ORC with IHE and OFOH		
ORC-turbine	$\dot{W}_{ORC\ Turbine} = \dot{m}_{33} h_{33} - (\dot{m}_{34} h_{34} + \dot{m}_{35} h_{35})$	$\dot{E}_{33} = \dot{E}_{34} + \dot{E}_{35} + \dot{w}_{orcturbine} + \dot{E}_{D,\mathrm{orcturbine}}$
Evap2	$\dot{Q}_{Evap2} = \dot{m}_7 (h_7 - h_8)$ $\dot{Q}_{Evap2} = \dot{m}_{32} (h_{33} - h_{32})$	$\dot{E}_7 + \dot{E}_{32} = \dot{E}_8 + \dot{E}_{33} + \dot{E}_{D,Evap2}$
IHE	$\dot{Q}_{IHE} = \dot{m}_{35} (h_{35} - h_{36})$ $\dot{Q}_{IHE} = \dot{m}_{29} (h_{30} - h_{29})$	$\dot{E}_{35} + \dot{E}_{29} = \dot{E}_{36} + \dot{E}_{30} + \dot{E}_{D,\mathrm{IHE}}$
TEG2	$\dot{Q}_{TEG2} = \dot{m}_{36} (h_{36} - h_{28})$ $\dot{Q}_{TEG2} = \dot{m}_{52} (h_{52} - h_{53})$	$\dot{E}_{52} + \dot{E}_{36} = \dot{E}_{53} + \dot{E}_{28} + \dot{W}_{TEG2} + \dot{E}_{D,TEG2}$
Pump2	$\dot{W}_{Pump2} = \dot{m}_{28} (h_{28} - h_{29})$	$\dot{E}_{28} + \dot{W}_{Pump2} = \dot{E}_{29} + \dot{E}_{D,\mathrm{pump2}}$
Pump3	$\dot{W}_{Pump3} = \dot{m}_{31} (h_{31} - h_{32})$	$\dot{E}_{31} + \dot{W}_{Pump3} = \dot{E}_{32} + \dot{E}_{D,\mathrm{pump3}}$
OFOH	$\dot{m}_{31} h_{31} = \dot{m}_{30} h_{30} + \dot{m}_{34} h_{34}$	$\dot{E}_{30} + \dot{E}_{34} = \dot{E}_{31} + \dot{E}_{D,\mathrm{OFOH}}$

To evaluate the system thermo-economically, the investment and operation and the cost rates of maintenance of each element should be determined. The sum of the investment cost rate and operation and maintenance cost rate is equal to the rate of total cost of the element, which are defined as [30]:

$$\dot{Z}_k = \dot{Z}_k^{CI} + \dot{Z}_k^{OM} \tag{5.a}$$

$$\dot{Z}_k^{CI} = \frac{CRF}{\tau} Z_k \tag{5.b}$$

$$\dot{Z}_k^{OM} = \frac{\gamma_k \, Z_k}{\tau} \tag{5.c}$$

where the parameter CRF indicates the capital recovery factor and the parameter τ indicates the working hours of the component per year. The capital recovery factor is calculated using the interest rate defined as [30]:

$$CRF = \frac{i_r \left(1+i_r\right)^n}{\left(1+i_r\right)^n - 1} \tag{6}$$

The total cost rate of the system is the sum of the cost rates of each component [30].

$$\dot{Z}_{tot} = \sum \dot{Z}_k \tag{7}$$

The other economic assumptions and assumed unit cost of products are given in Table 3.

Table 3. Input data associated with economic calculations

Parameter	Value	Unit
Fuel cost(C_f)	15.24	$/GJ
Interest rate(i)	0.12	-
Operation and maintenance factor (ϕ)	1.06	-
Number of years of operation(n)	20	year

2.4. Multi-objective optimization

Obtaining the best optimal operating condition is an essential part of the thermal systems analysis. Distinct objective functions exist which can be optimized together to assess the system best operating point, including exergy efficiencies, the net output power, the rate of chill production, and the sum of products unit exergy cost. Also, there are different methods and algorithms for multi-objective optimization procedure, including the genetics algorithm, the Grey wolf algorithm, etc. In the present research, a multi-objective optimization with total product unit cost, net output power, and exergy efficiency as the objective functions using the Grey wolf algorithm is applied and the data required for the optimization procedure are trained in the MATLAB software using machine learning method [31,32]. The key decision parameters and their bounds considered for the optimization are represented in Table 4.

2.5. Performance analysis

$$\eta_I = \frac{\dot{W}_{net,tot} + \dot{m}_{16}\left(h_{16} - h_{17}\right) + \dot{m}_{43} h_{43}}{\dot{m}_1\left(h_1 - h_9\right)} \tag{8.a}$$

$$\eta_{II} = \frac{\dot{W}_{net,tot} + \left(\dot{E}_{17} - \dot{E}_{16}\right) + \dot{E}_{43}}{\left(\dot{E}_1 - \dot{E}_9\right)} \tag{8.b}$$

$$C_{p,total} = \frac{\left(\dot{Z}_{total} + \dot{C}_{fuel}\right)}{\dot{W}_{net,tot} + \left(\dot{E}_{17} - \dot{E}_{16}\right) + \dot{E}_{43}} \tag{8.c}$$

The thermodynamic tool used for modeling the proposed multigeneration system from 4E perspectives is EES software.

3. Results and discussion

3.1. Model validation

To validate and evaluate the accuracy of the system modelling, the findings obtained from the performance assessment of the individual units of the present system and the reported findings in the relevant papers are compared.

3.1.1. Single flash geothermal system

The main and significant parameters resulting from the thermodynamic evaluation of the geothermal cycle, including exergy and energy efficiencies, the exergy destruction rate, and the net generated power rate, have been compared with paper [28]. Figure 2 compares the results achieved in the current study and reported in the reference paper. It can be seen that, for all parameters, the results obtained from the modelling have an acceptable match compared to the reference paper. The highest percentage of error is related to the exergy destruction rate, which is equal to 3.27%.

Table 4. Lower and upper bounds of the decision variables considered for multi-objective optimization

Parameter	Lower bound	Upper bound
T_1(K)	460	530
P_2(kPa)	500	1000
P_4(kPa)	40	200
ΔT_{HPG}(K)	5	20
ZT_M	0.6	1.6

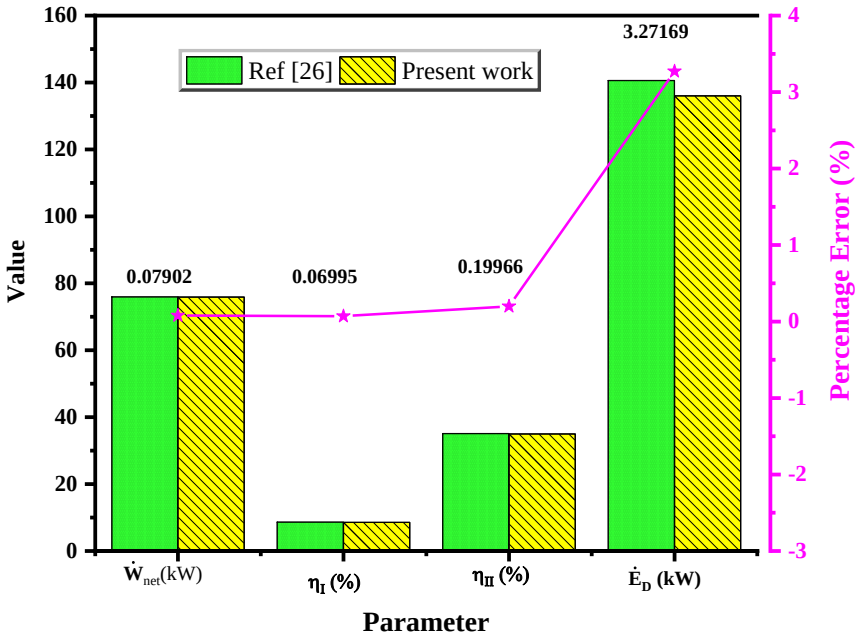

Fig. 2. Comparison of the results of geothermal cycle with the reference [26]

Table 5. Validation of the findings achieved from the present research against the reference for the DEAR system [29].

Component	symbol	Present work	Reference
HPG	Q_{HPG} (kJ)	251.6	252.407
Condenser	Q_{Cond} (kJ)	166.9	167.205
Evaporator	Q_{Eva} (kJ)	300	300
Absorber	Q_{Abs} (kJ)	384.7	385.236
Pump	w (kJ)	0	0
Coefficient of performance	COP	1.192	1.189

3.1.2. Double-effect lithium bromide/water absorption refrigeration configuration

Gomri and Hakimi [29] assessed the water-lithium bromide-based DEAR system from thermodynamic perspective. Table 5 shows the validation results of the main parameters of the absorption refrigeration system. This table clearly depicts that the evaluation of the system is done correctly and has acceptable accuracy.

3.1.3. ORC with the OFOH and the IHE

Table 7 summarizes the obtained results for the total generated power rate and energy efficiency for the ORC with the OFOH and compared them with the findings reported in the paper [29]. According to Table 6, there is a good match between the simulated findings and the reference paper results.

Table 6. Validation of the results obtained from the current study with the reference for the ORC with the IHE and the OFOH [29].

Parameter	Current work	Reference
$\dot{w}_{net}$(kW)	42.92	44.02
η_I(%)	15.02	15.35

Table 7. Important key parameter of the tri-generation system.

Parameter	Value
Exergy efficiency (%)	42.05
Net output power (kW)	134.7
Cooling load (kW)	88.67
Unit cost of product($/GJ)	77.8
Fresh water rate (kg/s)	0.109

3.2. Case study results

The key and main objective function of the studied system, consisting of the exergy efficiency, the net generated power rate, cooling load, the total product unit cost, and the produced freshwater mass flow rate, are given in Table 7.

Figure 3 displays the exergy destruction rate of each element of the proposed system. As mentioned earlier, the current system consists of four main units of the geothermal cycle, the DEAR system, the ORC with the OFOH and the IHE, and the HDH desalination system. The greatest exergy destruction belonged to the TEG1 among all components, which is 94.02 kW. Referring to this figure, the rate of system exergy destruction is 221.72 kW.

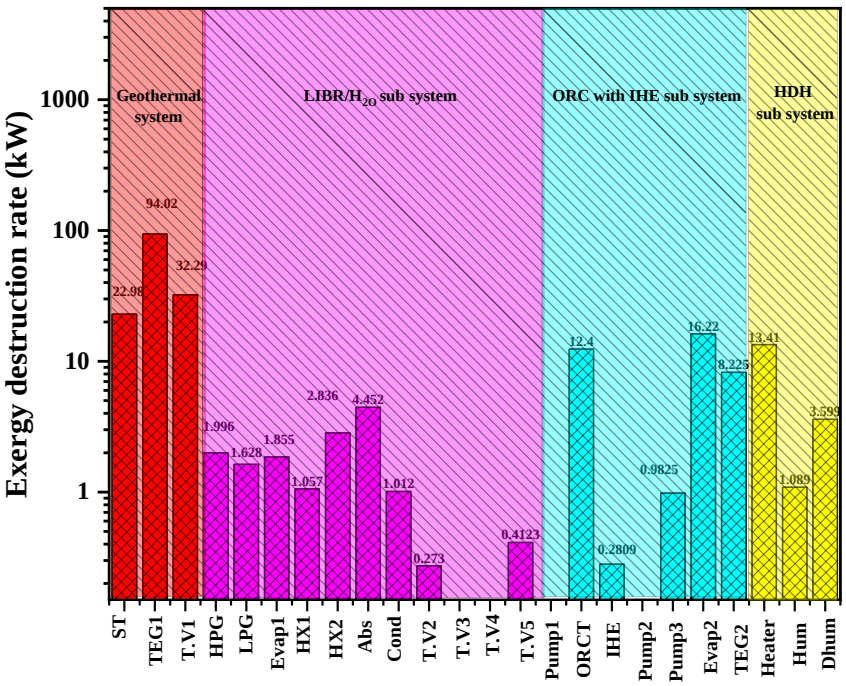

Fig. 3. Exergy destruction rate of the studied system for each component

3.3. Parametric study

3.1.3. The effects of geothermal inlet temperature

Figure 4 illustrates the effects of the geothermal inlet temperature on the system key parameters. Referring to Fig. 4, the exergy efficiency declines with the growth of the geothermal inlet temperature. This trend takes place since by rising the inlet temperature of the geothermal, the net generated power rate grows, but other useful productions of the system, including the produced freshwater mass flow rate and the cooling load, are reduced. However, as the increase rate of the net generated power rate is greater than others, it causes a growth in the system useful exergy production. It should be noted that with the rise of the system inlet temperature, the input exergy to the system also rises, and since this increase overcomes the growth of the system useful production, therefore, based on equation 8.b, the system exergy efficiency decreases from 49.76% to 38.66%. As mentioned above, a rise in the geothermal inlet temperature causes a decline in the cooling load. The reduction of heat in the HPG has a direct effect on reducing the cooling load and by rising the inlet temperature of the geothermal, the absorbed heat in the HPG reduces.

Since the fluid temperature difference in the water heater affects the produced freshwater mass flow rate directly, with the growth of the inlet temperature of the geothermal, the water heater temperature difference declines and ultimately leads to a reduction in the produced freshwater mass flow rate. Figure 4 also shows the variations of the total product unit cost. As can be observed, the total product unit cost decreases continuously with the growth of the geothermal inlet temperature due to the fact that the sum of the total cost rate relevant to the purchasing equipment and the consumed fuel and also the system useful products raise with the rise of the geothermal inlet temperature. As the growth rate of the useful products of the system is more than that for the sum of the total cost rate related to the purchasing equipment and the consumed fuel, therefore, according to equation 8.c, the total product unit cost reduces from 91.42 $/GJ to 73.07 $/GJ.

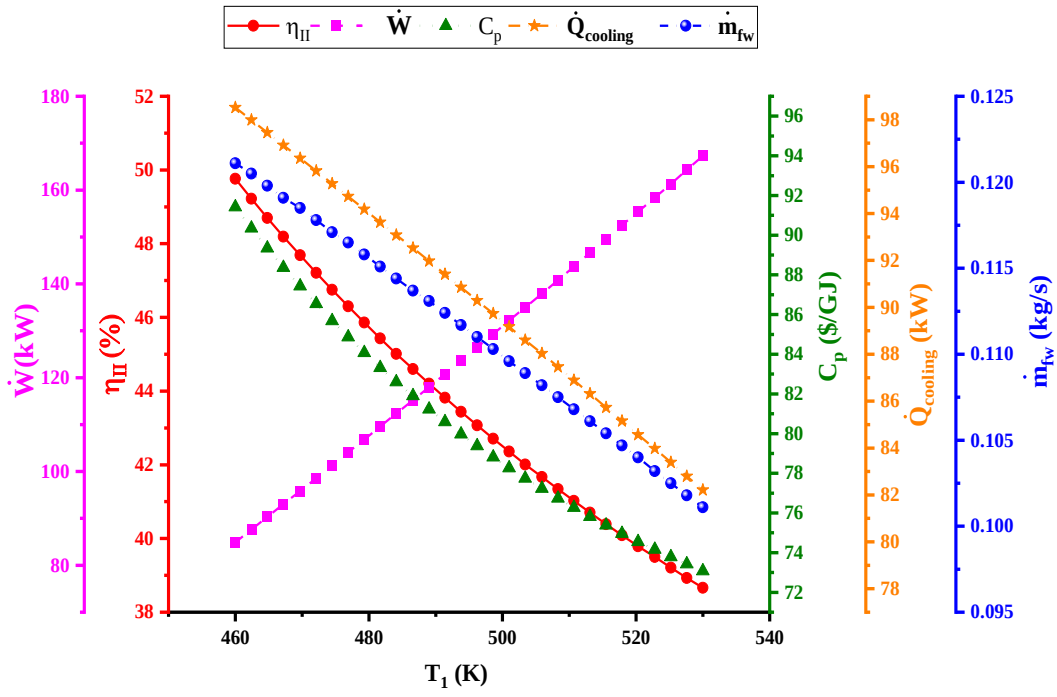

Fig. 4. The influence of geothermal inlet temperature on the η_{II}, $\dot{W}$, $\dot{Q}_{cooling}$, $\dot{m}_{fw}$, C_p

3.3.2. The effects of the flash chamber inlet pressure (P_2)

In Fig. 5, the variations of the system key parameters are shown in terms of the flash chamber inlet pressure. Referring to this figure, the exergy efficiency rises by rising of the flash chamber inlet pressure. This increasing trend occurs since the net generated power rate, cooling load, the produced freshwater mass flow rate, in general all the system useful products rise with the growth of flash chamber inlet pressure. On the other hand, the input exergy to the system also increases, but the increasing rate of the system useful products overcomes the increasing rate of the input exergy to the system resulting in a rise in the exergy efficiency.

As the inlet pressure of the flash chamber rises, the produced power in the steam-turbine grows due to the increase in the pressure difference. Also, by rising of the flash chamber inlet pressure, the heat absorbed in the evaporator 2 by the ORC fluid (isobutene) increases resulting in increasing the ORC-turbine inlet mass flow rate causing a rise in the produced power in the ORC-turbine. All these factors ultimately raise the system net generated power rate. So that the net generated power rate reaches 166.8 kW at pressure of 1000 kPa.

Figure 5 also displays the variations of the system cooling load. Since the inlet temperature of the HPG (state 6) grows with the increase in the pressure of state 6, which increases the absorbed heat in the HPG and affects the increasing of the cooling load. Referring to Fig. 5, when the flash chamber inlet pressure changes from 500 to 1000 kPa, the cooling load increases by about 9%.

The heat transfer rate in the HDH desalination system affects the rise of produced freshwater mass flow rate directly. As the flash chamber inlet pressure rises, the received heat by the water heater rises according to Fig. 5, as a result, the produced freshwater mass flow rate rises from 0.1068 kg/s to 0.1128 kg/s.

The effects of the flash chamber inlet temperature on the total product unit cost are also exhibited in Fig. 5. The sum of the cost rate relevant to the consumed fuel and purchasing equipment increases with rising the flash chamber inlet pressure. On the other hand, the useful exergy produced by the system, including the net generated power rate, exergy of the produced freshwater, rises. But the system useful products growth rate is more than the increasing rate of the sum of the cost rate of the consumed fuel and purchasing equipment causing reduction in the system total product unit cost.

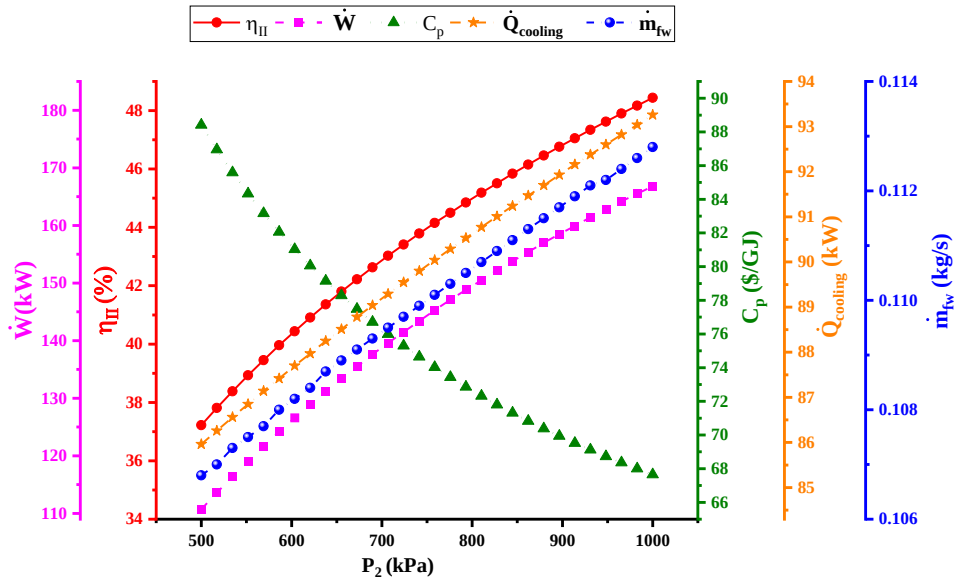

Fig. 5. The influence of *the* flash chamber inlet pressure on the η_{II}, $\dot{W}$, $\dot{Q}_{cooling}$, $\dot{m}_{fw}$, C_p

3.3.3. The effects of the steam-turbine outlet pressure (P_4)

The influence of the steam-turbine outlet pressure on the system objective functions is exhibited in Fig. 6. When the outlet pressure of the steam-turbine is the geothermal cycle downstream pressure and has no effect on the absorbed heat by the HPG and water heater, increasing of the steam-turbine outlet pressure has no effect on the cooling load and the produced freshwater mass flow rate, and these parameters remain unchanged.

Figure 6 also indicated the variations of the system exergy efficiency by increasing of the steam-turbine outlet pressure. Since the system input exergy is constant in this case, the most significant variable affecting the exergy efficiency is the useful produced exergy. By increasing the pressure of state 4, the power produced in the steam-turbine decreases due to the constant enthalpy of state 3 and enthalpy of state 4 leading to the reduction of the enthalpy difference in this unit. Reduction of the produced power in the steam-turbine results in a decline in the system net generated power rate resulting in decreasing the system exergy efficiency. When the steam-turbine outlet pressure are 40 and 200 kPa, the exergy efficiencies are 47.03% and 37.47%, respectively.

The changes of the total product cost are also displayed in Fig. 6. As stated in the previous part, the system useful exergy decreases with increasing the pressure of state 4 leading to increasing the total product unit cost according to equation 8.c. It should be noted that the cost rate of purchasing equipment also rises with the increase of the steam-turbine outlet pressure.

3.3.4. The influence of HPG temperature difference (ΔT_{HPG})

The trend of changing the significant and main objective functions of the investigated system, according to the temperature difference in the HPG, is exhibited in Fig. 7. According to this figure, growing the temperature difference in the HPG causes a decline in the system exergy efficiency. The reason for this decreasing trend is that the growth in the temperature difference in the HPG leads to a decline in the outlet temperature of the HPG (state 7) causing a reduction in the heat received in the evaporator 2. By rising the rate of heat absorption, the fluid mass flow rate entering the ORC-turbine decreases causing a decrease in the system total produced power, as a result, the useful produced exergy of the system reduces and due to the unchanged system input exergy, the overall system exergy efficiency declines.

The heat absorbed by the HPG affects the cooling load directly. Since the heat absorbed by the HPG rises with the growth in the HPG temperature difference, therefore, the cooling load also increases from 44.41 kW to 176.8 kW. Figure 7 also exhibits the effects of HPG temperature difference on the produced freshwater mass flow rate. The rise in the HPG temperature difference results in a rise of water heater heat transfer rate and rises the produced freshwater mass flow rate.

The effects of the HPG temperature difference on the total product cost is shown in Fig. 7. The sum of the total cost rate relevant to the purchasing equipment and the consumed fuel and the system useful exergy decrease as the HPG temperature difference grows. As the slope of the decreasing rate of the system useful exergy is greater than the slope of the decreasing rate of the sum of the total cost rate relevant to the purchasing equipment and the consumed fuel, the total product unit cost rises from 74.39 $/GJ to 85.41 $/GJ when the HPG temperature difference rises from 5 K to 20 K.

3.4. Multi-objective optimization results

As mentioned in the previous sections, the multi-objective optimization is carried out with different objective functions using machine learning method and Gray wolf method. Moreover, the TOPSIS approach is utilized to determine the optimized point. Based on the multi-objective optimization utilizing the Grey wolf algorithm, the Pareto frontiers are exhibited in Fig. 8. To optimize three objective functions of exergy efficiency, the total product unit cost, and the net generated power rate, the multi-objective optimization is conducted. The optimized values for the total product unit cost, the net generated power rate, and the exergy efficiency are 62.5 $/GJ, 180 kW, and 54%, respectively.

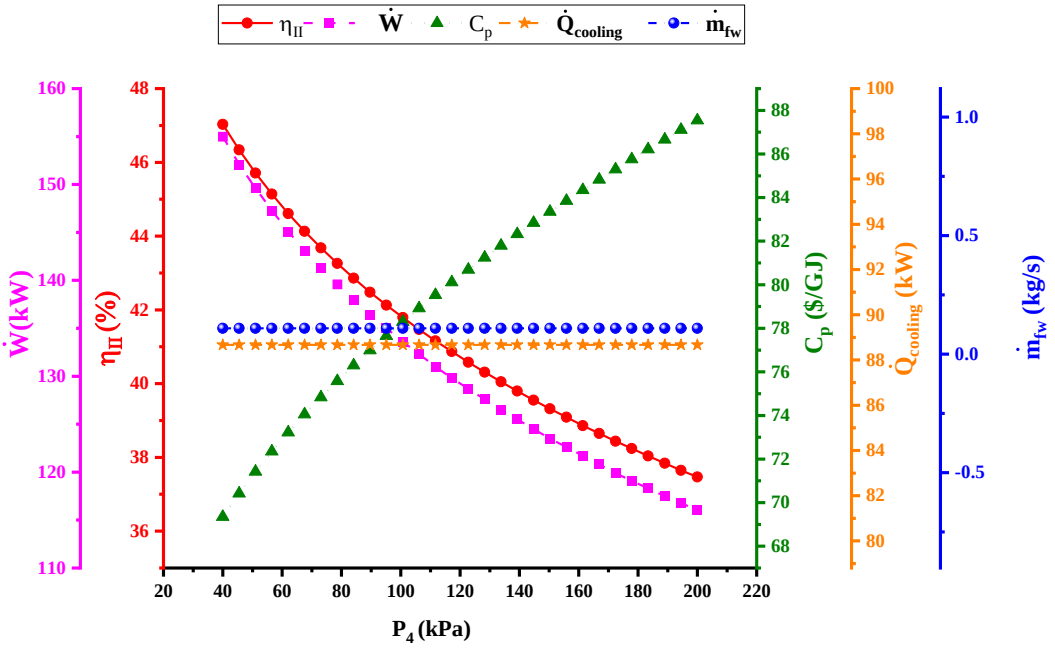

Fig. 6. The influence of *the* steam turbine outlet pressure on the η_{II}, $\dot{W}$, $\dot{Q}_{cooling}$, $\dot{m}_{fw}$, C_p

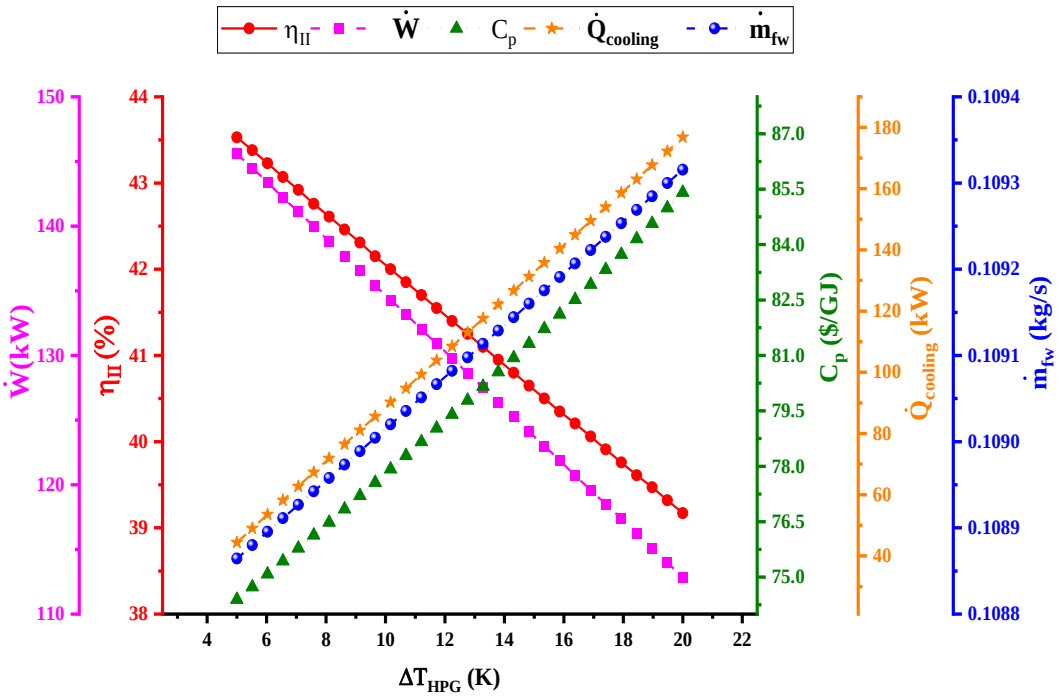

Fig. 7. The influence of the HPG temperature difference on the η_{II}, $\dot{W}$, $\dot{Q}_{cooling}$, $\dot{m}_{fw}$, C_p

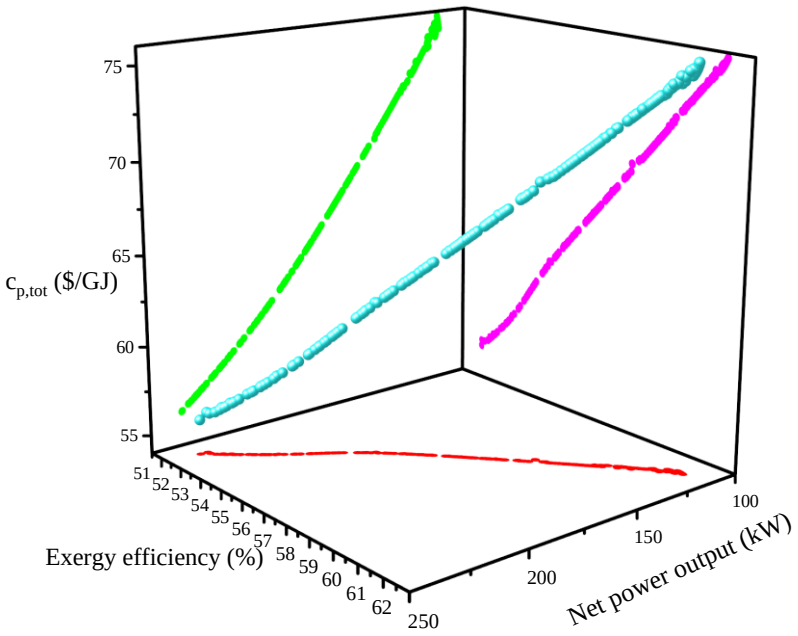

Fig. 8. Pareto frontier for multi-objective optimization

5. Conclusions

The novel multi-generation system powered by the geothermal energy is assessed from thermodynamic and economic aspects in the current work. This novel system consists of the geothermal cycle, the ORC with the OFOH and the IHE, HDH desalination system, and the DEAR system introduced to produce freshwater, power, and cooling load, which has not been stated in the other literatures.

To evaluate this tri-generation system under different working conditions, a comprehensive parametric evaluation is applied from thermodynamic and economic aspects. In addition, in order to achieve the optimized performance, the multi-objective optimization is applied utilizing the machine learning method and Gray wolf algorithm. The vitally important outcomes of this study are as follows:

- Under base design conditions, the system exergy efficiency and the total product unit cost are 42% and 77.8 $/GJ, respectively.
- The net generated power rate, cooling load, and the produced freshwater mass flow rate are reported 134.7 kW, 88.67 kW, and 0.109 kg/s, respectively.
- Among all studied system elements, TEG1 has the highest exergy destruction rate, which is 94.02 kW. Additionally, the overall system exergy destruction rate is 221.72 kW.
- According to parametric evaluation, the produced freshwater mass flow rate, the total product cost, and cooling load decrease with increasing the geothermal inlet temperature, however, the net generated power rate declines.
- With increasing the HPG temperature difference, the total product unit cost, the mas flow rate of the produced freshwater, and the cooling load increase, however, the net generated power rate and the exergy efficiency decrease.
- Under multi-objective optimization, the total product unit cost of the system, the net generated power rate, and the system exergy efficiency are 62.5 $/GJ, 180 kW, and 54%.

References

[1] Panwar, N., S. Kaushik, and S. Kothari, Role of renewable energy sources in environmental protection: A review.

Renewable and Sustainable Energy Reviews, 2011. 15(3): p. 1513-1524.
[2] Khanmohammadi, S., M. M. Baseri, P. Ahmadi, A. A. A. Al-Rashed, and M. Afrand Proposal of a novel integrated ocean thermal energy conversion system with flat plate solar collectors and thermoelectric generators: Energy, exergy and environmental analyses. Journal of Cleaner Production, 2020. 256: p. 120600.
[3] Mohtasham, J., Renewable energies. Energy Procedia, 2015. 74: p. 1289-1297.
[4] Alavy, M., P. Shirazi, and M.A. Rosen, Long-term energy performance of thermal caisson geothermal systems. Energy and Buildings, 2023. 292: p. 113152.
[5] Huang, J., A. Abed, S. Eldin, Y. Aryanfar, and J. Alcaraz, Exergy analyses and optimization of a single flash geothermal power plant combined with a trans-critical CO2 cycle using genetic algorithm and Nelder–Mead simplex method. Geothermal Energy, 2023. 11(1): p. 1-20.
[6] Wang, H., G. Yan, E. Tag-Eldin, R. Chaturverdi, Y. Aryanfar, J. Alcaraz, M. Amin, and H. Moria, Thermodynamic investigation of a single flash geothermal power plant powered by carbon dioxide transcritical recovery cycle. Alexandria Engineering Journal, 2023. 64: p. 441-450.
[7] Assad, M.E.H., Y. Aryanfar, S. Radman, B. Yousef, and M. Pakatchian, Energy and exergy analyses of single flash geothermal power plant at optimum separator temperature. International Journal of Low-Carbon Technologies, 2021. 16(3): p. 873-881.
[8] Fan, G., Y. Gao, H. Ayed, R. Marzouki, Y. Aryanfar, F. Jarad, and P. Guo, Energy and exergy and economic (3E) analysis of a two-stage organic Rankine cycle for single flash geothermal power plant exhaust exergy recovery. Case Studies in Thermal Engineering, 2021. 28: p. 101554.
[9] El Haj Assad, M., Y. Aryanfar, A. Javaherian, A. Khosravi, K. Aghaei, S. Hosseinzadeh, J. Pabon, and SMS. Mahmoudi, Energy, exergy, economic and exergoenvironmental analyses of transcritical CO2 cycle powered by single flash geothermal power plant. International Journal of Low-Carbon Technologies, 2021. 16(4): p. 1504-1518.
[10] Farshi, L.G., S. M. S. Mahmoudi, M. A. Rosen, and M. Amidpour, Exergoeconomic analysis of double effect absorption refrigeration systems. Energy Conversion and Management, 2013. 65: p. 13-25.
[11] Bagheri, B.S., R. Shirmohammadi, S. M. S. Mahmoudi, and M. A. Rosen, Optimization and comprehensive exergy-based analyses of a parallel flow double-effect water-lithium bromide absorption refrigeration system. Applied Thermal Engineering, 2019. 152: p. 643-653.
[12] Alali, A.E. and K. Al Khasawneh, Performance analysis of stirling engine double-effect absorption chiller hybrid system for waste heat utilization from gas turbine modular helium reactor. Energy Conversion and Management, 2022. 251: p. 114976.
[13] Zhang, F., Y. Yan, G. Liao, and E. Jiaqiang, Energy, exergy, exergoeconomic and exergoenvironmental analysis on a novel parallel double-effect absorption power cycle driven by the geothermal resource. Energy Conversion and Management, 2022. 258: p. 115473.
[14] Jiménez-García, J.C., I. Moreno-Cruz, and W. Rivera, Modeling of an Organic Rankine Cycle Integrated into a Double-Effect Absorption System for the Simultaneous Production of Power and Cooling. Processes, 2023. 11(3): p. 667.
[15] Yari, M. and S. Mahmoudi, A thermodynamic study of waste heat recovery from GT-MHR using organic Rankine cycles. Heat and Mass Transfer, 2011. 47(2): p. 181-196.
[16] Hung, T.-C., Waste heat recovery of organic Rankine cycle using dry fluids. Energy Conversion and Management, 2001. 42(5): p. 539-553.
[17] Seyed Mahmoudi, S.M., R. G. Sardroud, M. Sadeghi, and M. A. Rosen, Integration of Supercritical CO2 Recompression Brayton Cycle with Organic Rankine/Flash and Kalina Cycles: Thermoeconomic Comparison. Sustainability, 2022. 14(14): p. 8769.
[18] Karabuga, A., M.Z. Yakut, and Z. Utlu, Assessment of thermodynamic performance

of a novelty solar-ORC configuration based hydrogen production: An experimental study. International Journal of Hydrogen Energy, 2023.

[19] Ochoa, G.V., D.V. Castilla, and D.M. Casseres, Sensitivity analysis and multi-objective optimization of the energy, exergy and thermo-economic performance of a Brayton supercritical CO2-ORC configurations. Energy Reports, 2023. 9: p. 4437-4455.

[20] Javed, S. and A.K. Tiwari, Performance Assessment of Different Organic Rankine Cycle (ORC) Configurations Driven by Solar Energy. Process Safety and Environmental Protection, 2023.

[21] Nondy, J. and T. Gogoi, Exergoeconomic investigation and multi-objective optimization of different ORC configurations for waste heat recovery: A comparative study. Energy Conversion and Management, 2021. 245: p. 114593.

[22] Zhar, R., A. Allouhi, A. Jamil, and K. Lahrech, A comparative study and sensitivity analysis of different ORC configurations for waste heat recovery. Case Studies in Thermal Engineering, 2021. 28: p. 101608.

[23] Giwa, A., N. Akther, A. Al Housani, S. Haris, and S. Hasan, Recent advances in humidification dehumidification (HDH) desalination processes: Improved designs and productivity. Renewable and Sustainable Energy Reviews, 2016. 57: p. 929-944.

[24] Abbasi, H.R., H. Pourrahmani, and N. Chitgar, Thermodynamic analysis of a tri-generation system using SOFC and HDH desalination unit. International Journal of Hydrogen Energy, 2021.

[25] Qasem, N.A., Waste-heat recovery from a vapor-absorption refrigeration system for a desalination plant. Applied Thermal Engineering, 2021. 195: p. 117199.

[26] Feili, M., H. Ghaebi, T. Parikhani, and H. Rostamzadeh, Exergoeconomic analysis and optimization of a new combined power and freshwater system driven by waste heat of a marine diesel engine. Thermal Science and Engineering Progress, 2020. 18: p. 100513.

[27] Musharavati, F., S. Khanmohammadi, A. H. Pakseresht, and S. Khanmohammadi, Enhancing the performance of an integrated CCHP system including ORC, Kalina, and refrigeration cycles through employing TEG: 3E analysis and multi-criteria optimization. Geothermics, 2021. 89: p. 101973.

[28] Yari, M., Exergetic analysis of various types of geothermal power plants. Renewable Energy, 2010. 35(1): p. 112-121.

[29] Gomri, R. and R. Hakimi, Second law analysis of double effect vapour absorption cooler system. Energy conversion and management, 2008. 49(11): p. 3343-3348.

[30] Bejan, A., G. Tsatsaronis, and M.J. Moran, Thermal design and optimization. 1995: John Wiley & Sons.

[31] Mahmoudi, S.M.S., E. Gholamian, and N. Ghasemzadeh, Recurrent machine learning based optimization of an enhanced fuel cell in an efficient energy system: Proposal, and techno-environmental analysis. Process Safety and Environmental Protection, 2023. 173: p. 414-425.

[32] Javaherian, A., N. Ghasemzadeh, N. Javanshir, M. Yari, M. Vajdi, and H. Nami, Techno-environmental assessment and machine learning-based optimization of a novel dual-source multi-generation energy system. Process Safety and Environmental Protection, 2023.